Atmospheric Research 192 (2017) 58–71

Contents lists available at ScienceDirect

Atmospheric Research

journal homepage: www.elsevier.com/locate/atmosres

Sensitivity analysis of WRF model PBL schemes in simulating boundary-layer variables in southern Italy: An experimental campaign

E. Avolio[a,*], S. Federico[b], M.M. Miglietta[c], T. Lo Feudo[a], C.R. Calidonna[a], A.M. Sempreviva[d]

[a] Institute of Atmospheric Sciences and Climate - National Research Council (ISAC-CNR), Lamezia Terme, Italy
[b] Institute of Atmospheric Sciences and Climate - National Research Council (ISAC-CNR), Roma, Italy
[c] Institute of Atmospheric Sciences and Climate - National Research Council (ISAC-CNR), Lecce, Italy
[d] Technical University of Denmark, Department of Wind Energy, Roskilde, Denmark

ARTICLE INFO

Keywords:
WRF model
Planetary boundary layer (PBL)
PBL parameterization schemes
Experimental campaign
Wind lidar

ABSTRACT

The sensitivity of boundary layer variables to five (two non-local and three local) planetary boundary-layer (PBL) parameterization schemes, available in the Weather Research and Forecasting (WRF) mesoscale meteorological model, is evaluated in an experimental site in Calabria region (southern Italy), in an area characterized by a complex orography near the sea. Results of 1 km × 1 km grid spacing simulations are compared with the data collected during a measurement campaign in summer 2009, considering hourly model outputs.

Measurements from several instruments are taken into account for the performance evaluation: near surface variables (2 m temperature and relative humidity, downward shortwave radiation, 10 m wind speed and direction) from a surface station and a meteorological mast; vertical wind profiles from Lidar and Sodar; also, the aerosol backscattering from a ceilometer to estimate the PBL height.

Results covering the whole measurement campaign show a cold and moist bias near the surface, mostly during daytime, for all schemes, as well as an overestimation of the downward shortwave radiation and wind speed. Wind speed and direction are also verified at vertical levels above the surface, where the model uncertainties are, usually, smaller than at the surface. A general anticlockwise rotation of the simulated flow with height is found at all levels. The mixing height is overestimated by all schemes and a possible role of the simulated sensible heat fluxes for this mismatching is investigated. On a single-case basis, significantly better results are obtained when the atmospheric conditions near the measurement site are dominated by synoptic forcing rather than by local circulations.

From this study, it follows that the two first order non-local schemes, ACM2 and YSU, are the schemes with the best performance in representing parameters near the surface and in the boundary layer during the analyzed campaign.

1. Introduction

The thermo-dynamic structures in the lower troposphere are among the principal sources of forecast inaccuracy in mesoscale models (Stensrud, 2007; Hu et al., 2010). Simulating these features properly is essential for improving forecasts and for simulating weather phenomena related to the processes in the planetary boundary layer (PBL), the portion of the lower atmosphere directly affected by the surface exchange of moisture, heat and momentum (Stull, 1988; Stensrud, 2007). The evolution of the thermo-dynamic and kinematic structures in the lower troposphere is strongly influenced by the behavior of turbulent eddies, which mostly work at spatiotemporal scales usually not resolved by mesoscale models. Consequently, these unresolved turbulent phenomena are expressed via PBL parameterization schemes (Stull, 1988; Holton, 2004).

The planetary boundary layer height (PBLH, or mixing height) is often identified as the height of the inversion level separating the free troposphere from the boundary layer (Stull, 1988). This region is usually defined as the lowest (1–3 km thick) region of the atmosphere, characterized by friction and turbulent mixing phenomena; the latter plays an important role in the exchange of energy with the upper atmospheric layers, and work as a feedback mechanism in wind circulation. Consequently, the PBL plays an important role in air pollutants mixing and dispersion, and should be properly represented

* Corresponding author at: ISAC-CNR, Area Industriale compartment 15, 88046 Lamezia Terme, CZ, Italy.
E-mail address: e.avolio@isac.cnr.it (E. Avolio).

http://dx.doi.org/10.1016/j.atmosres.2017.04.003
Received 16 December 2016; Received in revised form 20 March 2017; Accepted 3 April 2017
Available online 04 April 2017

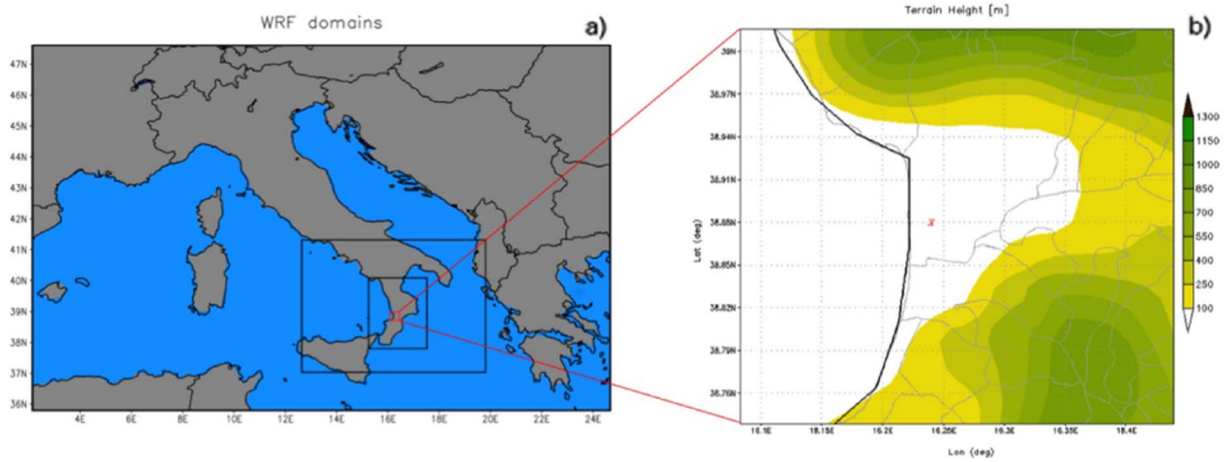

Fig. 1. (a) The four WRF domains; (b) 1 km spacing WRF grid (orography). A red cross denotes the Lamezia Terme experimental site. (For interpretation of the references to color in this figure legend, the reader is referred to the web version of this article.)

in air quality studies that use numerical weather prediction models as drivers. The correct representation of the PBL is also crucial for the accurate forecast of severe weather phenomena: the accurate simulation of the evolution of a thunderstorm, for example, requires a proper representation of moisture, vertical lift, atmospheric instability, wind shear, etc. (Johns and Doswell, 1992), which depend on the transport of moisture, heat and momentum in the PBL.

For the Calabria region, our test-site in southern Italy (Fig. 1), the role of PBL is crucial, mainly considering the particular micro-climatic characteristics of the Mediterranean basin and the specific geomorphological features of the territory. The nearby Ionian and Tyrrhenian seas often act as instability sources, providing moisture and heat which have contributed to the occurrence of numerous floods and landslides in the recent years (Federico et al., 2003a, 2003b, 2008). Additionally, the land-sea circulations interact with the complex orography, whose small-scale features are difficult to disentangle numerically, even at very high horizontal resolutions (Gascon et al., 2016).

Several studies have investigated the role of the PBL parameterization schemes in atmospheric flow-field simulations, both for air quality purposes and for the analysis of severe weather events. Most of these studies is primarily focused on mid-latitude continental regions, in particular the United States (Shin and Hong, 2011; Zhong et al., 2007; Hu et al., 2010; Cohen et al., 2015), or on tropical areas (Xie et al., 2012; Hariprasad et al., 2014). Also in Europe, some authors have examined the role of PBL schemes in simulating the main surface parameters (Borge et al., 2008; Banks et al., 2016), with particular attention to the wind characteristics (Floors et al., 2013; Kleczek et al., 2014; Miglietta et al., 2013; Kim et al., 2013; Draxl et al., 2014). The results of these studies show that there is not an optimal WRF PBL scheme in all cases, but the performance varies depending on the parameters considered and on the atmospheric conditions.

Differently from most of the earlier studies, mainly related to flat, mid-latitude continental regions, this paper deals with a complex orographic area. Here, in particular, five PBL parameterization schemes are tested during a measurement campaign performed in summer 2009, from July 15 to August 6, with the purpose of evaluating the WRF model sensitivity to the PBL parameterizations and to the land-surface interactions, which play a crucial role in the simulation of the meteorological variables in the lower troposphere. The large set of available meteorological data, ranging from surface measurements to vertical profiles, represents a pretty unique opportunity for model validation in the area.

The paper is organized as follows. Section 2 describes the WRF model setup, the observations used to evaluate the model performance, the relevant statistical parameters as well as the methodologies to estimate the height of the boundary layer; a general description of the main meteorological conditions during the campaign is also provided. Section 3 shows the results of the performance evaluation; Section 4 provides a brief summary and the conclusions.

2. Model, observations and methodology

The main purpose of the measurement campaign was to analyze the boundary layer variables at Lamezia Terme coastal site (Fig. 1) during different weather conditions in summertime. The experimental site is located on the west coast of the Calabria Peninsula, in southern Italy, 600 m from the coastline. The region is surrounded by the Tyrrhenian Sea (west) and by the Ionian Sea (east and south). The Apennines Mountains separate the coasts, reaching 2000 m of maximum elevation.

Several instruments were deployed in the experimental site, ranging from standard surface meteorological stations to acoustic and optical remote sensing tools. The use of different instruments, based on different principles of detection, was adopted for inter-calibration procedures, as well as to reach a better understanding of the physical processes responsible for the evolution of the PBL variables.

Hourly data are considered for measurements; thus, the number of records included in the verification is 552 (23 days × 24 h). For the verification, the “nearest neighbor” approach is adopted. Hereafter, we shortly describe all the available instrumentation, before focusing on the comparison with the WRF model output.

2.1. WRF model

In this work, we used the WRF-ARW model (Skamarock et al., 2008) version 3.4.1 to simulate the local scale flow and PBL characteristics during the measurement campaign. Four two-way nested domains were used (Fig. 1a) with varying horizontal grid resolutions. The parent domain covers the central Mediterranean basin (27 km grid spacing in both NS and WE directions; 70 × 50 grid points). The first nested grid represents the southern Italian Peninsula (9 km grid spacing; 67 × 52 grid points). The second nested grid is centered over the Calabria region (3 km grid spacing; 64 × 82 grid points). Finally, the innermost higher resolution grid (1 km grid spacing; 31 × 31 grid points) covers the surroundings of the Lamezia Terme experimental site (Fig. 1b); this very high resolution is adequate to resolve most mesoscale features in this complex study area.

Initial and boundary conditions were obtained from the National Center for Environmental Prediction - Global Forecast System (NCEP-GFS) analyses (0.5-degree horizontal resolution); high-resolution global sea surface temperature analyses from NCEP were also considered for the WRF model initial/boundary conditions.

For an optimal management of the computational resources, the

model was implemented with 28 terrain-following vertical levels; they are not equally spaced since nearly half of them are within the boundary layer. This configuration, using a quite coarse vertical resolution, is due to an optimal management of the computational resources finalized to an operational use of the model. For each day, a 36-h simulation starting at 12:00 UTC was performed and the first 12-h were considered as spin-up time; hourly outputs were generated.

In order to test the impact of the vertical resolution we performed additional simulations for two days, one dominated by the synoptic forcing and the other in breeze conditions (these are the two regimes found during the campaign, see Section 2.4), using 49 vertical levels, obtaining that the results do not change significantly for all parameters.

The main physical parameterizations used in this study include the new Rapid Radiative Transfer Model (RRTMG) longwave radiation scheme (Iacono et al., 2008), the Goddard shortwave radiation scheme (Chou and Suarez, 1999), the Noah land-surface model (Tewari et al. 2004), the single-moment 5-class microphysics scheme (WSM5; Hong et al. 2004) and the Kain–Fritsch cumulus parameterization (Kain 2004), the latter being activated only for the coarser two grids.

Five different PBL schemes were adopted, with their associated surface layer, in order to evaluate the sensitivity of the model to different schemes in simulating the main atmospheric parameters in the boundary layer. A brief description of the selected schemes follows in the next section.

2.1.1. PBL schemes

The PBL parameterizations tested in this paper consist of two non-local (YSU, ACM2) and three local (MYNN2, MYJ, QNSE) closure schemes. The difference between these two groups is related to the extension of the region that is able to affect the PBL variables at one point. For local closure schemes, only the vertical layers symmetrically adjacent to a specific point are able to directly affect the variables at that point; in contrast, non-local schemes are able to consider also variables in a deeper layer, including multiple vertical levels (Stensrud, 2007).

Also, the calculation of the PBL height is different between the two categories: (a) in the first category (non-local schemes), the PBL height is calculated as the lowest level, located above a certain pre-determined minimum height, at which the bulk Richardson number (Ri_b) exceeds a certain threshold. For these first-order schemes, no additional prognostic equation is required to express the effects of turbulence on the mean variables. (b) The second category (local schemes) determines the PBL height as the level where the turbulent kinetic energy (TKE) profile decreases to some pre-defined threshold values.

The Yonsei University (YSU) scheme (Hong et al. 2006) is a first-order, non-local scheme with an explicit entrainment layer and a parabolic K-profile in an unstable mixed layer. It is a modified version of the MRF scheme (Hong and Pan 1996) used in MM5 model (Dudhia 1993). With respect to MRF, in the YSU scheme the explicit treatment of the entrainment processes is introduced. The PBL height is determined from the Ri_b method, i.e. considering the level where the surface simulated Ri_b exceeds a critical threshold.

The Asymmetrical Convective Model version 2 (ACM2) scheme (Pleim 2007) is a first-order, non-local closure scheme that represents non-local upward mixing and local downward mixing. It is a modified version of the ACM1 scheme of the MM5 model. The scheme has an eddy-diffusion component in stable conditions, in addition to the explicit non-local transport in unstable conditions by the ACM1 scheme. The PBL height is defined as the height at which Ri_b, calculated above the level of neutral buoyancy, exceeds a critical value.

The Mellor–Yamada–Janjic (MYJ) scheme (Janjic 2002) is a 1.5-order prognostic TKE scheme with local formulation to determine the eddy diffusion coefficients and the vertical mixing; it is a modified version of the old Eta scheme from the MM5 model (Janjic 1990). The PBL height is determined from the value of TKE as the level at which the TKE profile decreases to a small prescribed value. This scheme is generally appropriate for all stable and slightly unstable flows.

The Quasi-Normal Scale Elimination (QNSE) scheme (Sukoriansky et al. 2005) is a 1.5-order, local closure scheme; it has an option to account for wave phenomena within stable boundary layers. The PBL height is defined as the height at which TKE decreases to a prescribed low value. The scheme is generally efficient for stable stratification and weakly unstable conditions.

The Mellor–Yamada–Nakanishi–Niino level-2.5 (MYNN2) scheme (Nakanishi and Niino 2006) is a 1.5-order, local closure scheme. Here, the stability and the mixing length are based on the results of large eddy simulations to surmount the typical biases associated with other Mellor-Yamada type schemes (underestimation of TKE and convective layer growth). The MYNN2 scheme predicts sub-grid TKE terms, and the PBL height is determined as the height at which TKE falls below a critical value.

Beside the PBL schemes, it is necessary to define an appropriate surface layer. This determines the surface exchange coefficients in order to calculate the sensible and latent heat fluxes and the momentum flux. Each PBL parameterization used here has a corresponding surface-layer scheme in the WRF model. A summary of the five PBL schemes adopted and the associated surface-layer schemes is shown in Table 1.

2.2. Near surface measurements

For the validation of the simulations performed with the WRF model during the campaign, the data from several instruments were used. These include:

– A surface meteorological station (ADCON TELEMETRY) operated routinely during the campaign. Data are available every 10 min. The measured surface parameters are: 2 m temperature (T), 2 m relative humidity (RH), global radiation (RAD), 10 m wind speed (WSP) and 10 m wind direction (WDIR).

– A 10-meter meteorological mast to monitor the main surface meteorological parameters and, specifically, to estimate turbulence. The mast was equipped with a METEK USA-1 sonic anemometer for the measure of turbulent fluxes, a fast response Hygrometer from NOAA, sensors (Risoe-DTU in-house) for the measure of temperature difference DT between different heights, i.e. T5 m–T2 m and T10 m–T2 m, an absolute temperature sensor (Risoe-DTU in-house) at 10 m, a cup anemometer and wind vane for the measure of wind speed and direction at 10 m. All the instruments are located in the experimental field of CNR-ISAC in Lamezia Terme.

For the verification of the WRF model we have considered T, RH and RAD measurements from the surface station; WSP and WDIR data,

Table 1
Summary of the PBL schemes used.

PBL scheme	Closure order	Surface layer scheme	PBL height method	Threshold
Yonsei University (YSU)	1.0 non-local	Monin–Obukhov	Rib method	0.0/0.25
Asymmetric Convective Model version 2 (ACM2)	1.0 non-local	Monin–Obukhov	Rib method	0.25
Mellor–Yamada–Janjic (MYJ)	1.5 local	Eta similarity	TKE threshold	0.2 $m^2 s^{-2}$
Quasi-Normal Scale Elimination (QNSE)	1.5 local	QNSE	TKE threshold	0.01 $m^2 s^{-2}$
Mellor–Yamada–Nakanishi–Niino level 2.5 (MYNN2)	1.5 local	MYNN	TKE threshold	1 × 10–6 $m^2 s^{-2}$

instead, are taken from the ultrasonic anemometer, due to its better quality and accuracy in the measurement. However, to check their consistency, first we compared the 10 m wind speed measurements from the surface station with that of the mast; the results show a good agreement (coefficient of correlation $R = 0.95$ for a time-series of 552 hourly recorded data).

2.3. Vertical profiles measurements

Several advanced ground-based remote sensing instruments (optical and acoustic) were employed during the campaign for the vertical sounding of the PBL parameters. Each instrument is characterized by specific features and peculiar utilizations; their simultaneous use can be helpful for inter-comparison operations and for better understanding turbulence phenomena. These are:

– Wind Lidar (Windcube WLS7-0012, LEOSPHERE): this instrument is a pulsed Doppler Lidar, operating at the eye-safe 1.5 μm wavelength, set to measure wind speed and direction every 10s at 10 heights, ranging from 40 m to 250 m.

– Sodar (DSDPA.90-24, METEK): it is an acoustic sounder that provides wind and turbulence vertical profiles in the lower troposphere. The instrument operates in the range 45 m–405 m heights with a working frequency of 1280 Hz. Sampled data are averaged every 10 min.

– Ceilometer (CL31, VAISALA): this instrument is set to measure the total aerosol backscatter coefficient every 10s with a 20 m vertical resolution within the height range 20–7500 m. The wavelength of the laser is 905 nm, with the energy of 1.2 μJ per pulse. For eye-safety reasons, the laser pulse of the ceilometer is not very powerful. Data are collected at a frequency of 10 s.

Wind lidar and sodar were used for wind vertical profile measurements; ceilometer was employed for the PBL height estimation. All the instruments described above, as well as the surface stations, are located in the CNR-ISAC headquarter in Lamezia Terme, with a mean reciprocal distance of about 10 m.

For the evaluation of the WRF model in simulating vertical profiles, we consider wind speed and direction both from wind lidar and sodar. Nevertheless, wind data from lidar are preferred, due to their better quality and accuracy in measurement; furthermore, during the campaign there were some missing data and/or outliers for the sodar.

Before performing statistical analysis and commenting on the results, we have compared wind measurements from the two different remote sensing instruments for each vertical level, in order to verify their agreement (see in the Section 3.2.1).

2.3.1. PBL height estimation from ceilometer

In order to study the evolution of the boundary layer vertical structure and its height (PBLH), we used the ceilometer data collected during the campaign; this instrument presents some advantages to estimate PBLH, in particular its high temporal frequency and vertical range, as well as the possibility of relatively continuous operations. Since aerosol concentration is in general lower in the free atmosphere, PBLH can be associated with a strong gradient in the vertical backscattering profile.

Several methods are widely used to determine PBLH. In the simple Threshold Method (Münkel and Räsänen, 2004; Melfi et al., 1985), the mixing height is determined when the backscatter signal falls below a threshold value. In the widely used Gradient Method (Endlich et al., 1979; Münkel and Räsänen, 2004; Sicard et al., 2004; Emeis & Schafer, 2006; Emeis et al., 2008), the estimate of PBLH is achieved by identifying the altitude with the minimum backscatter gradient.

The method adopted in this work is an extension of the Gradient Method, i.e. the Idealized Backscatter Method (IBM), originally described by Steyn et al. (1999). In this procedure, the mixing height h is not calculated directly from the observed backscatter profile but from an idealized backscatter profile $B(z)$, fit to the measured profile by the equation:

$$B(z) = \frac{B_m + B_u}{2} - \frac{B_m - B_u}{2} erf\left(\frac{z - h}{\Delta h}\right) \quad (1)$$

where the error function *erf(x)* is defined as $\mathrm{erf}(x) = \left(\frac{2}{\sqrt{\pi}}\right)\int_0^x e^{-t^2}dt$, B_m is the mean mixing layer backscattering coefficient, B_u is the mean backscattering coefficient in the layer above the mixing height, and h is proportional to thickness of the entrainment layer covering the PBL in convective conditions.

In the idealized case in which the backscatter above the mixing layer and inside the mixing layer have constant values, B_u and B_m respectively, PBLH is defined as the height of the middle of the aforementioned entrainment layer. A detailed description of the methods is in Steyn et al. (1999), Eresmaa et al. (2006) and Emeis et al. (2008).

In this work, we evaluate the capability of WRF model in simulating the boundary layer structure, in particular we consider the sensitivity of the model with respect to five different PBL schemes. To achieve this goal, we considered the hourly PBL heights calculated with the IBM method for the days and hours in which the method could be applied, which correspond to 13 days (in the remaining days, the instrument has been inactive either for technical problems or for the occurrence of several fires in the surroundings, which might distort the interpretation of the backscattered aerosol profiles).

2.4. Meteorological conditions during the campaign

In this section, we give a general description of the synoptic conditions during the experimental campaign. This analysis provides a preliminary assessment of the prevailing meteorological conditions during various time periods within the campaign inclusive dates and facilitates the identification of suitable case studies.

In describing the synoptic weather conditions during the campaign, we have taken into account the GFS fields used to initialize the WRF model. To describe the conditions at the measuring site, the data collected by the available instruments, more specifically the surface weather station, were also considered.

First of all, we shortly describe the typical microclimatic and wind conditions at the Lamezia Terme site, located on the west coast of the Calabria Peninsula; the morphology of the region offers peculiar conditions for breeze development and convergence. The coastal flow regime is characterized by prevailing synoptic and sea-breeze winds coming from the same direction (west); furthermore, sea and land breezes might act in phase with up-slope and down-slope winds to determine stronger and more persistent breeze systems (Federico et al., 2010).

Also, the region is located near the center of the Mediterranean where the atmospheric pressure field can often determine calm synoptic conditions (Trigo et al., 1999; Bolle, 2003), especially in summer and fall (Colacino et al., 1997): these conditions may favor the development of local thermally-forced circulations.

The measurement campaign lasted 23 days, from 15 July to 6 August 2009. The weather conditions will be discussed considering groups of consecutive days. To easily identify the specific daily atmospheric situations, we report in Fig. 2 the time series of the surface parameters for the whole study period, and in Fig. 3 (a,b,c,d,e) the synoptic maps representative of each group of consecutive days. For brevity, only one map for each group is reported, i.e. the mean fields calculated at 12 UTC for all the days belonging to each group.

From day-by-day analysis of the campaign, we found that westerly winds are the predominant synoptic conditions for the whole period. These are due to the persistence of large-scale structures such as the Icelandic low, weakly oscillating between the North Atlantic Ocean and the North Sea, and the Azores high in the Southern Mediterranean. This configuration, remaining almost stationary, forces the flow from WNW,

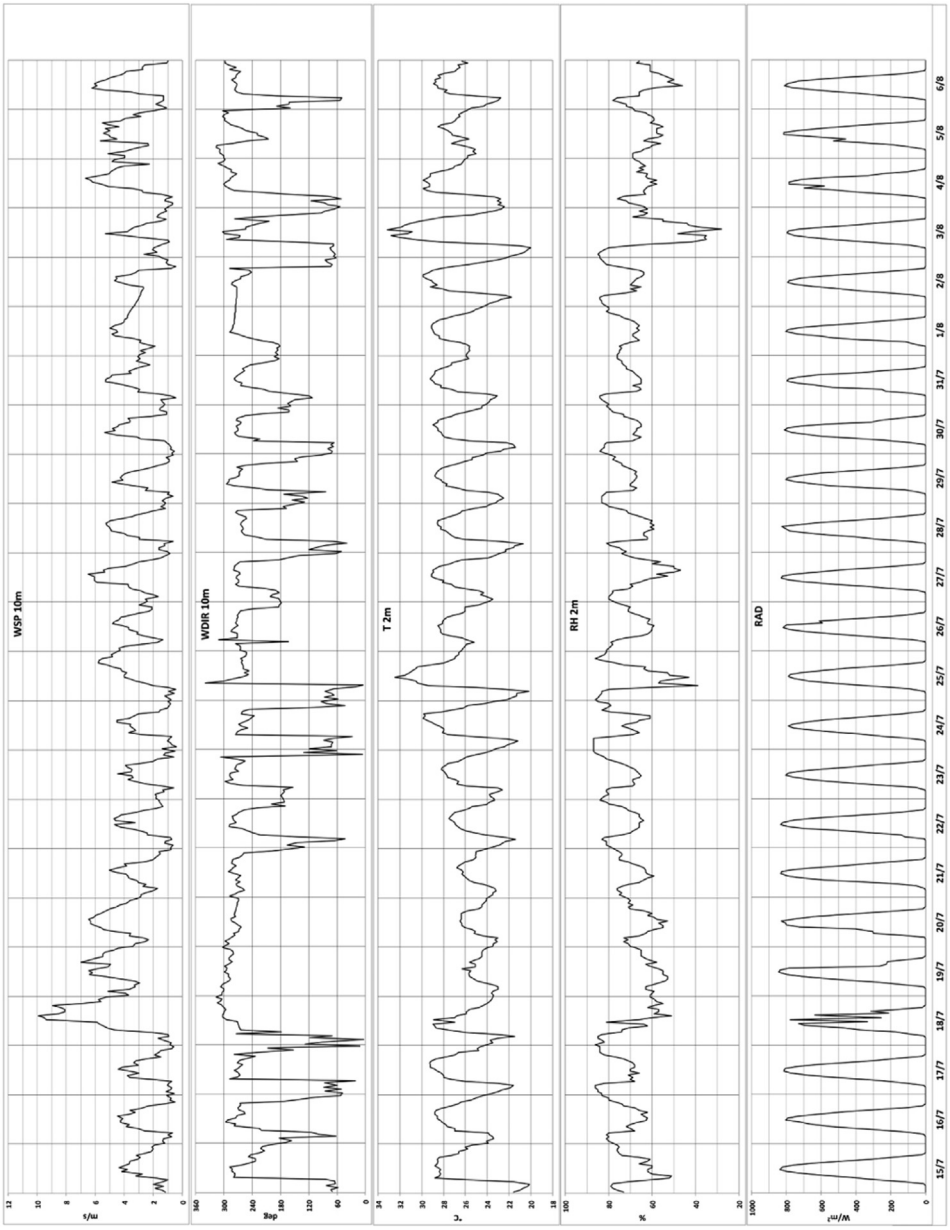

Fig. 2. Time series of surface parameters for the whole measurement campaign. From top to bottom: 10 m wind speed (m/s), 10 m wind direction (deg), 2 m temperature (°C), 2 m relative humidity (%), global radiation (W/m^2). On the x-axis are reported the days of the measurement campaign in the "day/month" format; vertical lines stand for 00 UTC.

both at high vertical levels and at the surface, with the wind intensity modulated by the position of the synoptic patterns.

We identified three main classes of atmospheric conditions, mainly related to the surface wind characteristics at the Lamezia Terme site: "sea/land breeze" (the wind is directed from the west during the day and from the east at night), "synoptic flows" (or "undeveloped breeze") (predominant westerly winds also at night; the land breeze is not able to develop and the flow at Lamezia Terme is directed from W-NW for the whole day) and "partially developed breeze" (an intermediate situation in which the sea breeze occurs during daytime, but the land breeze does not develop during nighttime and winds are mainly directed from south).

2.4.1. 15-16-17-18 July

The synergistic action of the Icelandic low and of the Azores high drove winds from N-NW over the Italian Peninsula; a secondary low pressure was present over the Black Sea. At the surface, the winds were weak-moderate during the first three days (values lower than 4 m/s). On July 18, there was a sudden change in the weather conditions; synoptic flows became stronger and oriented from W, due to the deepening of the low-pressure over the North Sea. The winds at the surface reached 13 m/s, the maximum value achieved for the whole campaign. Cloud cover and light rain occurred in the central hours of the day (July 18 was the only day in which rainfall - 1 mm - was recorded at this site).

2.4.2. 19-20-21 July

The Icelandic low slightly deepened and moved northward in the North Atlantic Ocean, so that the westerly flows became weaker. The Azores high-pressure was present over the Mediterranean, with a ridge extending over Italy. At the surface, the maximum wind speed decreased from 7 to 4 m/s; also, the surface temperatures slightly decreased.

2.4.3. 22-23-24-25-26-27 July

The upper-level flows were still from the west and relatively weak.

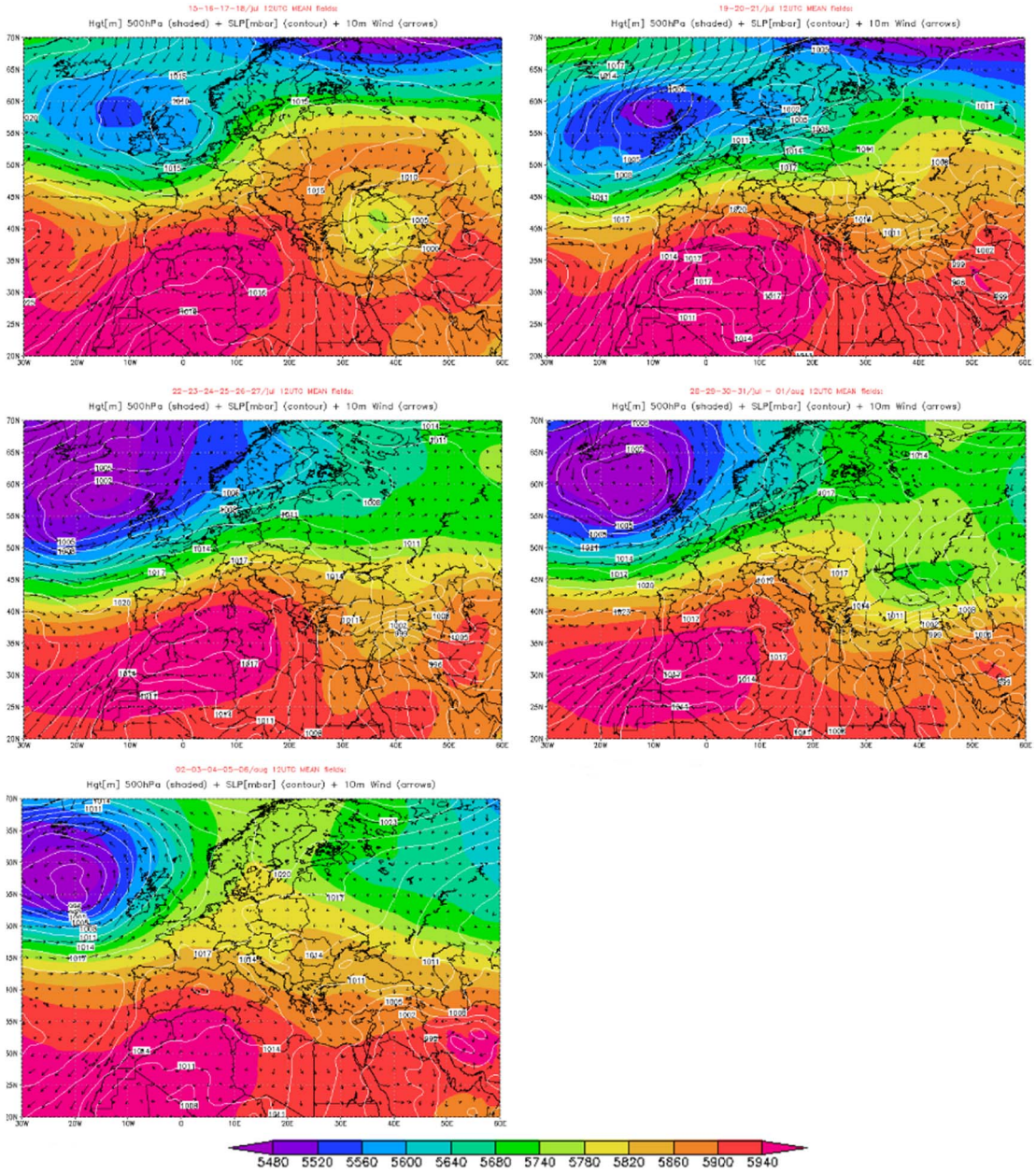

Fig. 3. Mean synoptic maps for five groups of consecutive days (mean values at 12 UTC for each group): (a) 15, 16, 17, 18 Jul; (b) 19, 20, 21 Jul; (c) 22, 23, 24, 25, 26, 27 Jul; (d) 28, 29, 30, 31 Jul, 1 Aug; (e) 2, 3, 4, 5, 6 Aug. The maps show: sea level pressure [hPa] (filled contours), geopotential height at 500-hPa [m] (contours), and 10-m winds (arrows).

Synoptic conditions were quite similar to those of the previous period, with a general broadening of the low-pressure and a further anticyclonic reinforcement on July 25 in the Mediterranean. The surface temperatures rose steadily during the four days as well as the wind speed. July 25 was the day (with August 3) when the highest temperatures were recorded (> 32 °C), while the surface winds exceeded 6 m/s.

2.4.4. 28-29-30-31 July–1 August

Persistent winds from the North-West were observed in the Mediterranean Basin, and the Azores high slowly moved to South-West. At the surface, the winds and surface temperatures did not exceed 5 m/s and 29 °C, respectively.

2.4.5. 2-3-4-5-6 August

Conditions of leveled mean sea level pressure persisted over the Mediterranean Basin, whereas westerly flows were still driven by the low-pressure over the North Atlantic Ocean. Sea level pressure values significantly decreased, consistently with the weakening and southward retreat of the Azores high. At the surface, temperatures gradually grew; on August 3, they reached the highest value observed during the entire experiment (> 33 °C), with winds exceeding 6 m/s.

From the analysis of the surface conditions, we can group the days into three main classes:

– "breeze": 15, 16, 17, 18, 22, 24, 25, 28, 29, 30 July and 2, 3, 4, 6 August (61% of total cases).

– "synoptic flows": 19, 20, 21 July (13% of total cases).

– "partially developed breeze": 23, 26, 27, 31 July and 1, 5 August (26% of total cases).

In the next section, we deepen the study and the statistics considering the whole measurements campaign; whereupon, as an additional digression, we also analyze the meteorological cases of "breeze" and of "synoptic flows" conditions.

2.5. Metrics used for the validation

The basic statistical indicators, adopted in this work to evaluate the model performances, were defined as follows (Wilks, 2011):

Mean Bias (MB):

$$MB = \frac{1}{N}\sum_{i=1}^{N}(FOR_i - OBS_i)$$

Root Mean Square Error (RMSE):

$$RMSE = \sqrt{\frac{1}{N}\sum_{i=1}^{N}(FOR_i - OBS_i)^2}$$

Pearson correlation index (R):

$$R = \frac{\sum_{i=1}^{N}(FOR_i - \overline{FOR})\bullet(OBS_i - \overline{OBS})}{\left(\sqrt{\sum_{i=1}^{N}(FOR_i - \overline{FOR})^2}\right)\bullet\left(\sqrt{\sum_{i=1}^{N}(OBS_i - \overline{OBS})^2}\right)}$$

with FOR: simulated field; OBS: observed field; N: number of records.

Daily MB is also calculated to study the daily-averaged performances in simulating the main surface parameters (see the next section).

3. Results and discussion

3.1. Surface meteorological parameters

WRF near-surface meteorological parameters were validated against the observations collected during the campaign. Results are presented for all considered variables and for each PBL scheme adopted, in terms of RMSE, MB and R. The meteorological variables taken into account for the verification are: 2 m temperature (T), 2 m relative humidity (RH), downward shortwave radiation (RAD), 10 m wind speed (WSP) and 10 m wind direction (WDIR).

3.1.1. The entire campaign period

The campaign-averaged performance statistical indicators, for the surface meteorological variables and for each WRF PBL scheme, are reported in Table 2. Metrics in the table have been computed considering the entire experimental campaign period, namely taking into account hourly data (simulations vs. observations) for 23 days (N = 552 records are considered).

Table 2
Statistics for the whole measurement campaign.

Variable	Scheme	R	MB	RMSE
T 2 m (°C)	YSU	0.77	− 0.39	1.63
	QNSE	0.77	− 0.71	1.72
	ACM2	0.78	− 0.35	1.59
	MYNN2	0.74	− 0.53	1.75
	MYJ	0.74	− 0.57	1.76
RH 2 m (%)	YSU	0.46	1.14	11.41
	QNSE	0.38	2.69	13.15
	ACM2	0.57	0.10	10.69
	MYNN2	0.39	1.81	12.73
	MYJ	0.32	1.56	12.99
RAD short (W/m^2)	YSU	0.98	86.06	135.73
	QNSE	0.98	87.82	135.77
	ACM2	0.99	88.27	134.59
	MYNN2	0.98	88.68	136.11
	MYJ	0.98	87.99	136.14
WSP 10 m (m/s)	YSU	0.74	1.25	1.84
	QNSE	0.81	0.95	1.54
	ACM2	0.68	1.16	1.89
	MYNN2	0.75	1.15	1.72
	MYJ	0.80	1.02	1.55
WDIR 10 m (°)	YSU	0.63	8.36	57.62
	QNSE	0.61	− 1.72	60.61
	ACM2	0.63	8.62	58.98
	MYNN2	0.59	7.12	60.15
	MYJ	0.64	4.61	57.93

From Table 2 it follows that all WRF PBL schemes show a cold and moist bias. The best performances belong to non-local schemes, in particular ACM2, followed by YSU, although all schemes provide pretty good results, especially for air temperature. For downward shortwave radiation, all schemes produce very similar results, with a general overestimation, but with an excellent correlation to the observations. This result is consistent with Avolio et al., 2016, where a general overprediction by above 100 W/m^2 was found at the Lamezia Terme site on a period of six-months. In contrast, the local schemes perform better for 10 m wind speed, the QNSE scheme being the best. All schemes overestimate the average wind speed by about 1 m/s. For the 10 m wind direction, the schemes behave similarly in terms of statistical score. The mean bias is positive for all schemes, except for QNSE, which means that the modeled wind is clockwise rotated with respect to observed wind.

For a better interpretation of the wind characteristics, we show the wind roses for each WRF PBL scheme and for the observed data (Fig. 4). All schemes are similar, simulating on average westerly winds (from the sea in Lamezia Terme); this result is in agreement with the observations, although the speeds appear overestimated. All WRF-PBL schemes simulate a small component from W-SW, which is absent in the mast wind rose, where a northwesterly component (mainly from WNW) is apparent. Only QNSE partially simulates the observed W-NW direction.

The overestimation of modeled wind speed has been reported in several recent works using WRF (Zhang et al., 2013; Hariprasad et al., 2014; Srikanth et al., 2015), as well as confirmed by previous studies at Lamezia Terme site using both WRF and RAMS models (Avolio et al., 2016). The cause of this overestimation may be tied to the difficulty to correctly simulate the sub-grid surface roughness and the related induced turbulence in the lower atmospheric levels (Jimenez and Dudhia, 2012).

Looking at the results, a significant cold and moist bias is apparent using the local schemes compared to the non-local schemes. At the same time, the non-local schemes overestimate wind speed more than the local ones. These results, in agreement with other similar studies (e.g., Miglietta et al., 2013; Kain, 2004; Cohen et al., 2015), are mainly associated to differences in the vertical mixing strength and entrainment of air from above the PBL. Non-local schemes, for their nature, are able to consider the effects of larger eddies on the dispersion of heat, moisture, and momentum throughout the PBL depth; for this reason, they generally simulate more accurately the diurnal-driven turbulence associated with the surface heating.

It is interesting to discuss the statistical significance of the differences among the PBL schemes, as well as their difference with observations. To study this point we use the Kolmogorov-Smirnov (K-S) test (Wilks, 2011), to assess if two datasets are drawn from the same distribution to a certain required level of statistical significance. For the K-S test, we considered all the values for the whole campaign (552 values, i.e. 24 h by 23 days) as a single distribution for each near-surface meteorological parameter (temperature, relative humidity, downward shortwave radiation, and wind speed).

The results of the K-S test for the differences of modeled and observed distributions show that the two datasets are different (99%, with the exception of the ACM2 for relative humidity, for which no differences are found) for all parameters. This result shows the difficulty to simulate surface parameters, in particular for the complex orographic conditions considered in this paper.

The tests for the difference of modeled distributions for different PBL schemes show that, with the exception of the downward shortwave radiation, there are differences between local and non-local schemes (95–99% depending on the parameter). However, the K-S test for the distributions of the meteorological parameters for local schemes (or for non-local schemes) shows that the distributions are different for RH

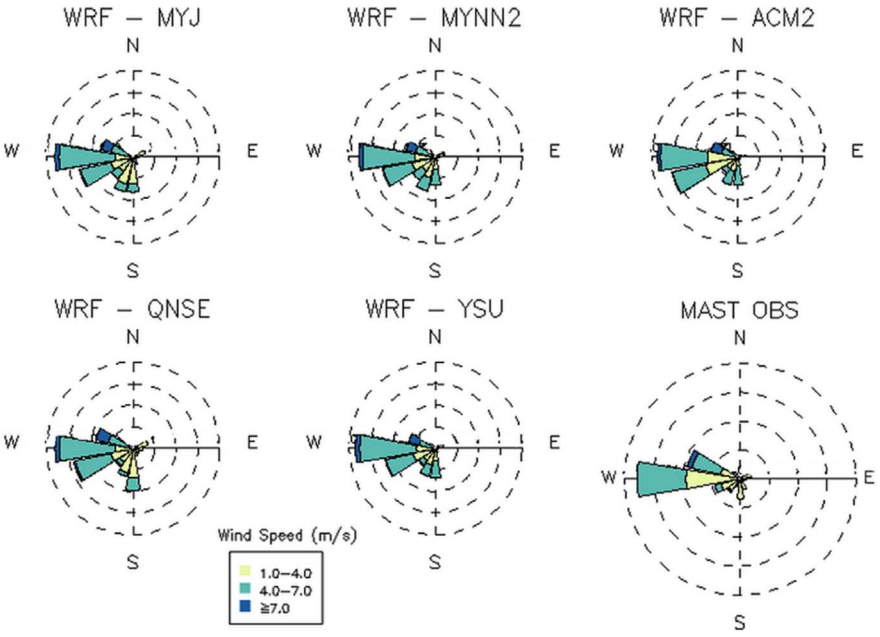

Fig. 4. Campaign-averaged wind roses for the different PBL schemes and for the meteorological MAST.

(95–99% depending on the schemes involved) but not for other parameters.

For the downward shortwave radiation, all the PBL schemes show similar distributions. This result is expected considering that clear skies were observed for most days of the campaign.

In summary, the applications of the K-S test to the distributions of surface parameters for different PBL schemes show that they are different between local and non-local schemes, while the difference between two local or two-non local schemes are less significant.

3.1.2. Hourly mean bias

To better understand the hourly dependence of the five WRF outputs in simulating the surface parameters, we report the hourly (time unit in UTC) MEAN BIAS in Fig. 5 (a,b,c,d).

For all schemes, the systematic cold (Fig. 5a) and moist (Fig. 5b) model biases noted in Table 2 are due to the daytime behavior, i.e. after 06 UTC. In contrast, during night-time the situation is reversed, showing a warm and dry bias. On average, the ACM2 scheme remains closer to the zero-bias line during daytime, while QNSE is the best scheme during the night. The lowest biases, both for temperature and for relative humidity, are recorded at 06 UTC, during the transition between the two different phases. In contrast, the maximum errors are at 16 UTC (MB between $-1.7\,^{\circ}C$ and $-2\,^{\circ}C$ for temperature and between 7% and 12% for relative humidity).

For the downward shortwave radiation (Fig. 5c), the performances of the PBL schemes are very similar. The overestimation reaches 200 W/m^2 at midday. Only from 06 to 12 UTC, when the solar irradiation increases in a significant way, small differences can be identified among the simulations. This is related also to the different surface layer schemes associated to each PBL parameterization.

The overestimation of the downward shortwave radiation may be related to some different physical mechanisms not properly simulated, e.g. the cloud coverage or the Aerosol Optical Depth (AOD). However, for the period considered in this work, clouds characterized only few days, and the cloud coverage was correctly reproduced, thus we believe that the simulation of AOD had a crucial role. In a similar framework, the study of Lara-Fanego et al. (2012) highlighted that the AOD was underestimated by WRF for Andalucia, Southern Spain, by comparing WRF AOD with MODIS/Terra Aerosol Daily L3 Global 1 Deg CMG data ($1 * 1^{\circ}$ spatial resolution). They also showed that the underestimation of AOD by 0.1–0.2 occurring in their simulations could explain the overestimation of 100 W/m^2 – 200 W/m^2. Finding the reason for the overestimation of the downward shortwave radiation is outside the scope of this paper, nevertheless we guess the AOD had a fundamental role in it and its impact will be considered in future studies.

Wind speed (Fig. 5d) is over-predicted by all WRF runs. During most of the hours, a large spread is present, with differences up to 1.5 m/s among the schemes. QNSE is the scheme fitting better the observations during night-time and in late afternoon, while ACM2 shows the lowest MB at noon (< 0.5 m/s). The relatively good performance of QNSE, as well as of the other local schemes, during conditions of greater atmospheric stability is in agreement with previous results (Shin and Hong, 2011; Hariprasad et al., 2014) comparing the two categories of PBL schemes.

Despite the overestimation of the downward shortwave radiation, all PBL schemes underestimate the temperature during the day; this may be determined by several factors such as the surface fluxes, the presence of clouds and aerosols, the wind speed. Fig. 5 suggests that the wind may exert some control also on the bias of other parameters. For example, the cold bias of surface temperature during daytime could be explained with the overestimation of surface wind, which, coming from the sea, brings relatively cold and moist air to the experimental site. If this advection is overestimated, a cold bias is expected, as shown in Fig. 5a. The wet bias (Fig. 5b) is also a consequence of the surface temperature underestimation.

3.1.3. The role of the synoptic forcing

In the following, we have briefly analyzed separately the cases of breeze and the synoptic flows, in order to highlight possible peculiarities associated with the specific atmospheric conditions. Statistics regarding T, RH, RAD and WSP are reported in Table 3. The results are discussed taking into account, as a benchmark, the campaign-averaged results in Table 2.

The WRF performances are slightly worse during the breeze cases than during the campaign-averaged results for all the PBL schemes. RMSE increases by about 8–15% for temperature and 4–12% for humidity, depending on the PBL scheme, the best performance being again that of ACM2. Differences in the shortwave radiation simulations are negligible (about 1% for all PBL schemes). For wind speed, RMSE increases in breeze conditions with respect to the whole campaign by < 10%; the best performances are for QNSE with RMSE of 1.66 m/s (versus 1.54 m/s in the whole campaign). For wind direction, no

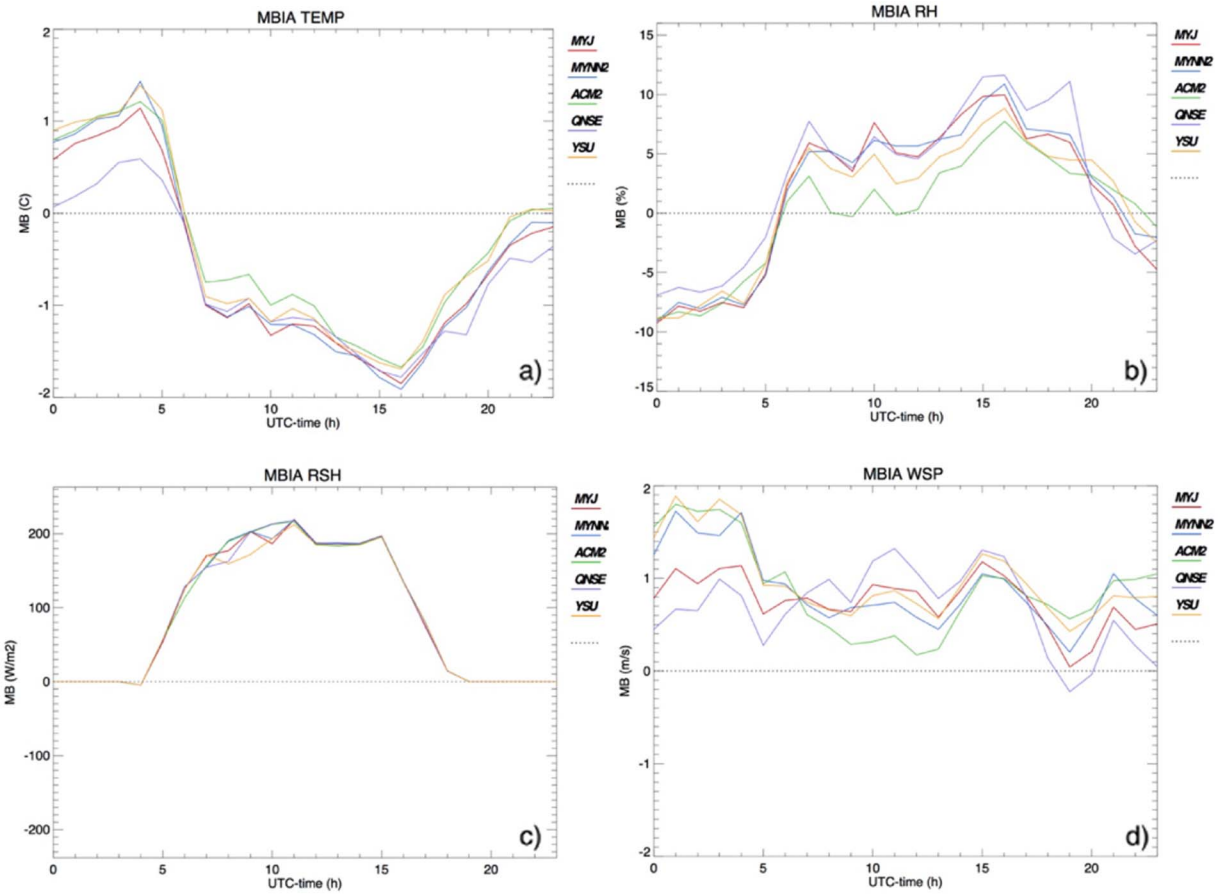

Fig. 5. Daily MB computed for the whole campaign and for the five PBL schemes as a function of hour (UTC) for: (a) 2 m temperature (°C); (b) 2 m relative humidity (%); (c) downward shortwave radiation at the surface (W/m^2); (d) 10 m wind speed (m/s). (For interpretation of the references to color in this figure legend, the reader is referred to the web version of this article).

substantial differences are recorded in terms of RMSE, while MB increases.

The analysis of the synoptic-flow-only cases shows that WRF performances are better than the average results during the whole campaign for all parameters and PBL schemes adopted. RMSE decreases by about 20–40% for temperature and 13–36% for relative humidity. Again, the best scheme is ACM2 and the worst QNSE. Also in this case, the differences for shortwave radiation are almost negligible. For wind speed, RMSE decreases by about 15–23% with respect to the whole campaign, with best performances by QNSE.

We remind the reader that breeze case study days represent more than half of the entire campaign, as previously discussed considering the micro-climatic characterization of the experimental site (Section 2.4); also, it is well known that the regional circulations represent very complex atmospheric patterns, especially near coastal sites, which partially explain the worse performances by WRF during such conditions. It is left for future plans to use a larger dataset in order to better quantify the performance of the WRF model at Lamezia Terme when the synoptic forcing is dominant compared to the breeze circulation.

The near-surface verification results presented here are in agreement with recent studies evaluating the model PBL schemes. Banks et al. (2016), in a similar experiment carried out over Greece, found a cold and moist bias by WRF (during daytime), concluding that the non-local schemes generally perform better. A strong overestimation of 10 m-wind speed also occurs for all considered schemes, and different scores are found in different synoptic situations. Hu et al. (2010) used three PBL schemes for a study over Texas regarding the WRF performances in reproducing the surface parameters. In agreement with our results, they discovered that the best performances are obtained with ACM2 and YSU schemes and found a general cold and moist bias.

3.2. Vertical wind profiles

3.2.1. LIDAR and SODAR measurements

As mentioned above, we have interpolated all WRF data at specific vertical levels for sake of comparison with wind lidar and sodar. The defined common levels are: 40, 60, 80, 100, 120, 140, 160, 180, 200, 250 m. First of all, we have compared wind measurements from the two different remote sensing instruments, level by level, to evaluate the agreement between them. Fig. 6a shows the vertical profile of R both for wind speed and direction, related to the whole measurement campaign. A high correlation is found, with values of $R > 0.8$ at lower levels for WSP (0.7 for WDIR). Above 180–200 m, the differences between the two instruments become higher and the correlation decreases, since the observational errors increase with the height.

Fig. 6b and c show the vertical profiles of RMSE between lidar and sodar (one measure is considered as the observation and the other as an estimation of it), for WSP and WDIR respectively, taking into account the three main categories defined above (all data, breeze cases, synoptic flows cases). Considering the results over the whole period, we can see that, below 180–200 m, RMSE values for wind speed are < 1.3 m/s; for WDIR, RMSE values are greater (around 40°) at lower levels, and slowly decrease to 30° at 200 m height. There are noticeable differences between the three categories of events. In the breeze cases, mainly for WDIR, the differences between the two instruments are significant; since breeze cases are 61% of the total, they significantly affect the campaign-averaged results (ALL case). For the synoptic flows, instead, we can observe a sensible reduction of the differences between the two

Table 3
Statistics for the surface meteorological parameters for the days characterized by the breeze circulation and synoptic-scale flows, for all the PBL schemes.

Variable	Scheme	BREEZE R	BREEZE MB	BREEZE RMSE	SYNOPTIC R	SYNOPTIC MB	SYNOPTIC FLOWS RMSE
T 2m (°C)							
	YSU	0.77	− 0.13	1.87	0.83	− 0.75	1.03
	QNSE	0.77	− 0.40	1.87	0.92	− 1.14	1.37
	ACM2	0.78	− 0.10	1.83	0.84	− 0.60	0.96
	MYNN2	0.73	− 0.19	1.97	0.90	− 1.13	1.28
	MYJ	0.74	− 0.20	1.95	0.91	− 1.18	1.33
RH 2m (%)							
	YSU	0.50	− 1.24	12.05	0.61	7.17	9.33
	QNSE	0.40	0.69	14.16	0.53	6.96	10.13
	ACM2	0.56	− 1.56	12.00	0.76	3.58	6.77
	MYNN2	0.45	− 0.60	13.39	0.64	8.82	10.61
	MYJ	0.39	− 1.33	13.57	0.49	8.90	11.20
RAD short (W/m^2)							
	YSU	0.98	83.46	137.78	0.98	92.10	140.55
	QNSE	0.98	86.33	137.21	0.98	93.44	143.08
	ACM2	0.98	87.38	135.91	0.98	92.67	142.03
	MYNN2	0.98	87.35	137.68	0.98	93.51	143.11
	MYJ	0.98	87.13	137.79	0.98	93.36	142.94
WSP 10m (m/s)							
	YSU	0.77	1.47	2.01	0.72	1.04	1.57
	QNSE	0.84	1.17	1.66	0.78	0.71	1.29
	ACM2	0.72	1.39	2.03	0.68	0.93	1.60
	MYNN2	0.78	1.38	1.88	0.77	0.80	1.31
	MYJ	0.84	1.25	1.68	0.78	0.70	1.24
WDIR 10m (°)							
	YSU	0.64	22.75	63.08	0.58	− 33.75	56.07
	QNSE	0.71	14.67	58.78	0.46	− 43.08	72.05
	ACM2	0.63	22.56	64.63	0.62	− 29.37	49.96
	MYNN2	0.61	22.89	65.80	0.63	− 36.18	56.36
	MYJ	0.67	20.12	61.88	0.59	− 34.75	61.15

instruments, which is particularly marked for WDIR.

3.2.2. Comparison between WRF and LIDAR wind profiles

As discussed above, lidar and sodar measurements are highly correlated, even if some small differences are found, mainly at higher levels. The mean model RMSE for wind speed, averaged over all vertical levels and all PBL schemes, is 1.5 m/s in comparison both with lidar and sodar. For wind direction, the mean RMSE is 44° with respect to lidar and 45° for sodar. Table 4 summarizes the comparison between the WRF outputs and both remote sensing instruments; only the RMSE statistics related to the whole period and to the average over all vertical levels are reported.

The results suggest that the statistical indices concerning the comparison of WRF model with lidar and sodar are almost identical; also, considering that several missing data and/or outliers were present

Table 4
RMSE averaged over all levels for the five PBL schemes, compared with Lidar and Sodar.

	YSU RMSE (m/s)	QNSE RMSE (m/s)	ACM2 RMSE (m/s)	MYNN2 RMSE (m/s)	MYJ RMSE (m/s)	Average RMSE (m/s)
WSP						
WRF vs LIDAR	1.3	1.8	1.2	1.4	1.6	**1.5**
WRF vs SODAR	1.4	1.7	1.4	1.4	1.6	**1.5**
WDIR						
WRF vs LIDAR	40	52	37	43	45	**44**
WRF vs SODAR	42	54	39	44	47	**45**

in the sodar dataset, the discussion about the WRF verification will be mainly focused on lidar measurements.

Fig. 7 (a-l) show: the campaign-averaged results (first row); the breeze case results (second row); the synoptic case results (third row); the first and second columns (RMSE and MB) are related to the wind speed while the third and fourth columns are related to the wind direction. The figure permits to compare easily the scores of the three different categories of events. To help interpreting the results, we have used the same scale for the horizontal axis, except for MB of WDIR in the synoptic cases (chart on the bottom right), because the values span a wider range than in the other cases.

For wind speed, the vertical profiles of RMSE are similar. This is particularly evident for the campaign-averaged and breeze cases, with errors ranging from 1.6 to 1.8 m/s, at all levels, for all schemes; only QNSE shows a larger RMSE. The profiles of RMSE show two relative maxima at 60–80 m and at 200 m, while for the breeze cases the peak of RMSE in the lower levels is evident only for a couple of schemes. The reduction of RMSE for the synoptic cases is notable. ACM2, the best scheme in this subset of cases, has a RMSE of about 1.2 m/s, while QNSE, the worst scheme, has an almost constant RMSE of about 1.8 m/s. Considering all levels, the two non-local ACM2 and YSU schemes perform better for wind speed (Table 4); this is more evident in the synoptic cases. Considering the mean bias of wind speed, results are slightly different. In the campaign-averaged case, we found that below 80 m four schemes have a negative, although small, bias; only YSU over-predicts the wind speed. In the upper levels, the bias is positive for all schemes. Averaging over all levels, the scheme with the smallest bias is QNSE, while YSU have the largest bias. Significant differences emerge between the cases of sea breeze and of synoptic flows; in the first case, a sensible over-prediction of wind speed is evident at all levels, while in the second case all schemes under-predict the wind speed at all levels.

Regarding the vertical profiles of wind direction, the RMSE

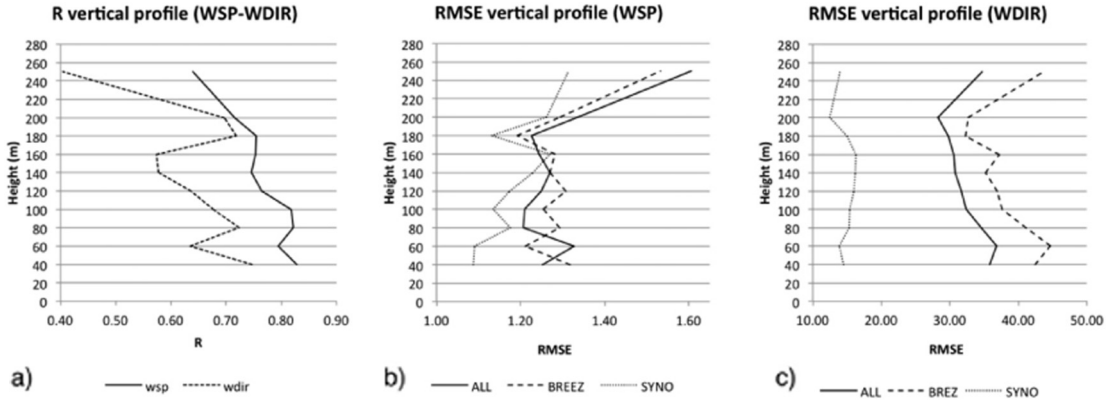

Fig. 6. (a) Coefficient of correlation between lidar and sodar; (b) vertical profiles of wind speed RMSE between lidar and sodar; (c) vertical profiles of wind direction RMSE between lidar and sodar.

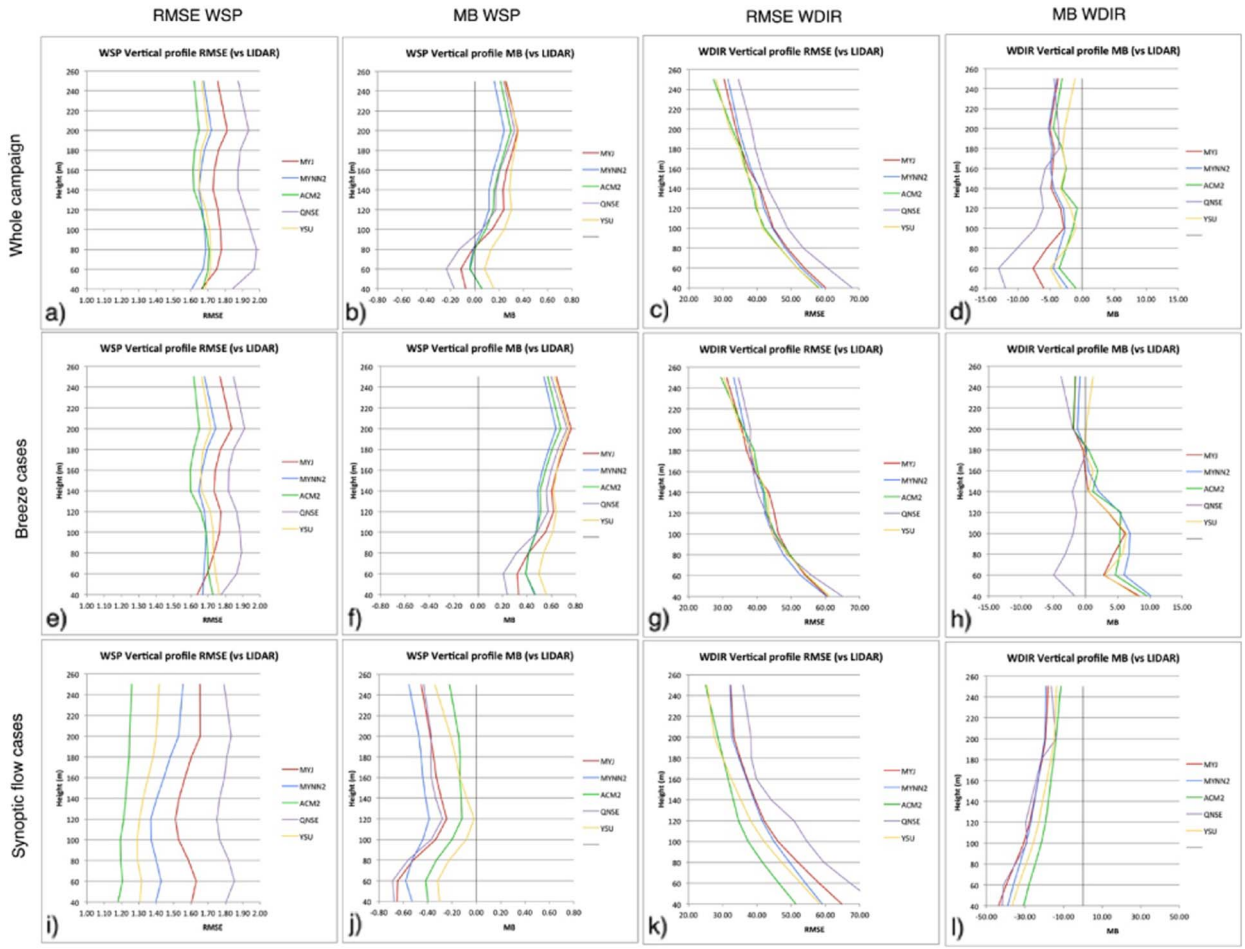

Fig. 7. Vertical profiles of RMSE and MB for wind speed and wind direction. (a) RMSE of wind speed for the whole campaign; (b) MB of wind speed for the whole campaign; (c) RMSE of wind direction for the whole campaign; (d) MB of wind direction for the whole campaign; (e), (f), (g), (h) are similar to (a), (b), (c), (d) but for the breeze cases; (i), (j), (k), (l) are similar to (a), (b), (c), (d) but for the synoptic flows cases. (For interpretation of the references to color in this figure legend, the reader is referred to the web version of this article).

decreases from about 60° at 40 m height to 30° at higher levels. The fact that the strongest error in wind direction is near the surface is due to the difficulty of the model to properly simulate the interactions in the surface layer. The profiles are similar for all the three categories of events and for all the schemes; only for the synoptic case a larger spread is noted among the schemes, with the values of RMSE generally larger than for the other two categories of events. For all the patterns, the two non-local schemes (ACM2 and YSU) have the smallest RMSE; QNSE, on average, is the worst scheme at all vertical levels.

The analysis of the mean bias reveals that, for the whole campaign, a general anticlockwise rotation of the simulated wind with respect the observed one is apparent for all PBL schemes. The minimum deviation is again obtained for the two non-local ACM2 and YSU schemes. The maximum deviation is associated with the QNSE scheme. The same behavior is also observed for the synoptic flow cases, but with much larger deviations (note the different horizontal axis spacing in the figure). In the breeze cases, the profiles are completely different: in fact, up to 180 m, almost all the schemes simulate a small clockwise rotation (positive bias), while only QNSE continues to have a negative bias. From these analyses it follows that, in days of synoptic flow, WRF simulates winds slightly rotated anticlockwise respect to the observations, whereas, in breeze days, WRF simulates winds with a slightly increased northerly component compared to the prevailing westerly observations.

3.3. PBL height

Usually, one of the variables most difficult to simulate with the mesoscale models is the PBL height. Here, the PBL height simulated with the WRF model is compared with the ceilometer estimates; in particular, the daily maximum PBL height (PBLH), which represents a critical information in turbulence and atmospheric instability studies, is estimated. The value of PBLH at 12 UTC is considered here, since it corresponds, on average, to the maximum value of the PBL height during daytime, very close to the time of maximum insolation at Lamezia Terme site. Also, the choice of this time permits to compare our results with analogous studies in which radiosoundings were available. Table 5 show the results for the days when the PBL height calculation from ceilometer was possible.

Because of the small statistical sample for the PBL height verification, only results relative to the whole campaign are reported, with no separation of breeze and synoptic flow cases. The Ceilometer observa-

Table 5
Mean PBLH for the different WRF PBL schemes, as well as for the ceilometer, at 12 UTC. The statistical sample consists of 13 records, which are the days when observations are available.

Variable	Scheme	Mean MAX PBLH
MAX PBLH (m) (12 UTC)	*CEILOM*	*527.27*
	YSU	592.91
	QNSE	1360.55
	ACM2	819.55
	MYNN2	463.27
	MYJ	718.36

Ceilometer data are indicated in italics.

Table 6
Statistics for the PBLH simulation by the different schemes for the daily hours (06–17 UTC).

Variable	Scheme	R	MB (m)	RMSE (m)
Daytime PBLH (m) (06–17 UTC)	YSU	0.36	-131.63	281.69
	QNSE	0.47	598.57	744.93
	ACM2	0.43	43.07	289.29
	MYNN2	0.20	-172.63	304.19
	MYJ	0.40	110.52	377.36

tions show that the maximum PBL height during the campaign is on average 527 m. Outputs with YSU and MYNN2 schemes are particularly close to this value (respectively 592 m and 463 m), whereas QNSE is almost three times as large. Also, the diurnal trend of the PBL heights simulated with the 5 different WRF PBL schemes is compared with the ceilometer estimation, taking into account the time interval from 06 UTC to 17 UTC. Table 6 summarizes the results. Regarding RMSE, the YSU and ACM2 schemes perform better; the ACM2 scheme has the minimum MEAN BIAS (43 m), while QNSE has the best correlation, which means that it is able to better capture the time variations, but, due to the strong bias, RMSE is very large.

A deeper interpretation of these results can be accomplished with Fig. 8, which shows the mean BIAS of PBLH, in the time interval 06 UTC–17 UTC, for the five WRF PBL schemes. It is confirmed that YSU and ACM2 are the WRF schemes with the minimum bias during the period, while YSU and MYNN2 present better results at 12 UTC (in accord with Table 5); the overestimation of PBLH by the QNSE scheme is apparent. Banks et al. (2015, 2016) found similar results, showing that the mixing height reproduced with the local QNSE scheme is overestimated for all the synoptic flow conditions, while Hariprasad et al. (2014) found that during stable morning conditions, the local closures produced deeper layers, in contrast to the non-local schemes. Following Banks et al. (2015) and Shin and Hong (2011), we suppose that the higher PBL heights simulated with the QNSE scheme may be due to the more intense daytime surface heat fluxes.

In agreement with the results for surface temperature and humidity, also for the mixing height estimation the best performances are obtained with non-local schemes, likely for a better simulation of the effect of the turbulence associated with the surface heating. Previous studies evaluating the PBL height with different WRF PBL schemes found results similar to those presented here. In fact, a large spread is often present among the various schemes, as well as a large difference between the simulated PBLH and the measured one. Banks et al. (2016) assessed that the minimum errors are obtained using the ACM2 scheme, mostly during daytime, while Breuer et al. (2014), testing five different WRF PBL schemes in Hungary, found an overestimation of the mixing height by about 500–1000 m.

3.4. The role of the sensible heat fluxes

As stated above, the differences in WRF model-simulated PBL heights are considerable. In particular, the QNSE scheme overestimates significantly PBLH, especially in the central hours of the day. This bias is relevant not only compared to the Ceilometer estimation, but also with respect to the other PBL schemes. At 12 UTC, the PBLH bias of QNSE is about 800 m with respect to the Ceilometer estimation and between 600 and 900 m with respect to the other PBL schemes. Since the PBL is strongly influenced by surface parameters, and in particular by surface fluxes of heat and moisture, the dependence of the fluxes on the PBL scheme (and on the corresponding surface layer) is investigated.

Fig. 9 shows the hourly surface sensible heat flux (HFX) averaged over all the days of the measurement campaign. The HFX values simulated by the QNSE scheme are much higher than those for the other schemes during daytime, with differences in the amplitude of the diurnal cycle > 100 W/m^2. Thus, the large overestimation of the PBL height by the QNSE scheme may be due to the higher surface heat fluxes simulated with this scheme. In fact, higher heat fluxes would lead to a highly convective atmosphere and to the growth of deeper daytime PBLs (Srikanth et al., 2015). The two non-local YSU and ACM2 schemes simulate the lowest HFX values compared to all the other schemes. Since such schemes are, on average, those with the best performance both in terms of surface measurements, low-level vertical profiles, as well as of PBL heights, we can infer that the sensible heat flux plays a key role in the performance of the WRF model at the local scale.

4. Conclusions

In the present study, we have evaluated the impact of five planetary boundary layer (PBL) parameterization schemes used in the Weather Research and Forecasting (WRF) mesoscale model for the simulation of the main atmospheric variables, directly related to the thermo-dyna-

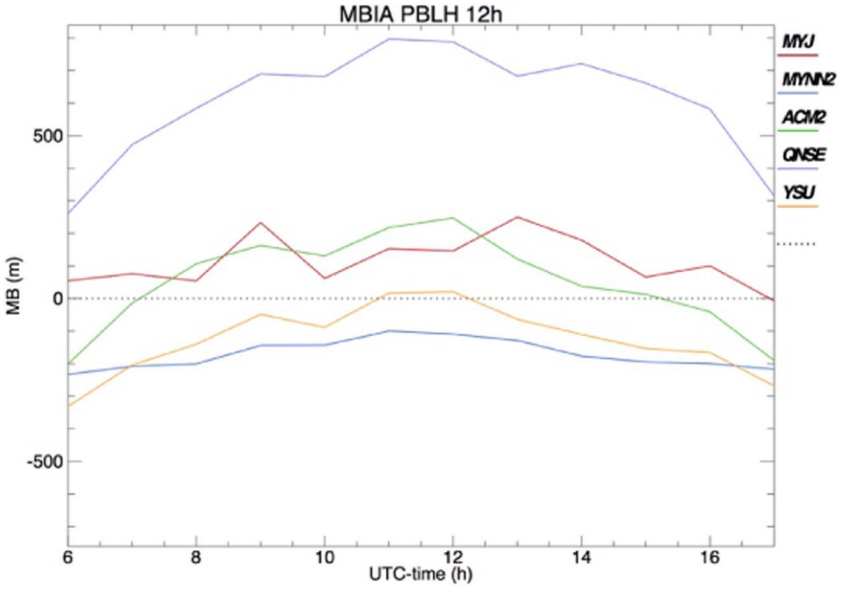

Fig. 8. MB for the PBLH for the whole campaign and for the five PBL schemes, for the daily hours (06–17 UTC). (For interpretation of the references to color in this figure legend, the reader is referred to the web version of this article).

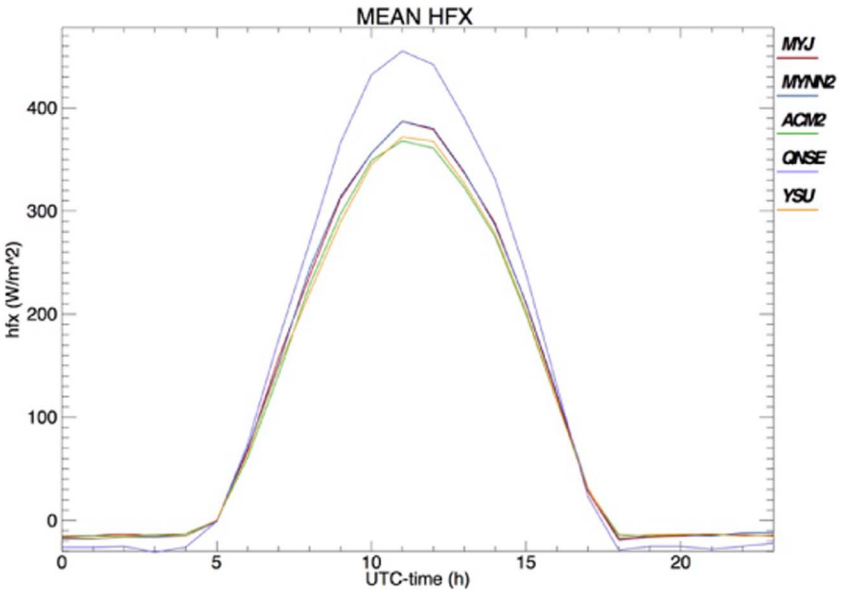

Fig. 9. Hourly values (UTC) of the sensible heat flux averaged over the whole campaign for the different PBL schemes. (For interpretation of the references to color in this figure legend, the reader is referred to the web version of this article).

mical behavior of the lower troposphere. A satisfactory representation of the boundary layer phenomena is crucial for an accurate simulation of air quality, as well as for adequate forecasts of severe weather phenomena. This study deals with a morphologically complex area in Southern Italy (Calabria region), where peculiar micro-climatic conditions are frequently recorded due to the rough coastline and the complex orography. The area of interest is the Lamezia Terme coastal site, and the model performances are evaluated during a measurement campaign conducted in summer 2009, from 15 July to 6 August.

Simulations were performed at high horizontal resolution (1 km) over the test-site, where several instruments were available for verification, ranging from a standard surface meteorological station to acoustic and optical remote sensing instruments. Near-surface observations of 2 m temperature, 2 m relative humidity, downward shortwave radiation, 10 m wind speed and direction were collected from a surface meteorological station and a 10 m meteorological mast; vertical wind profiles, from 40 m to 250 m, were measured by a wind Lidar and a Sodar; the aerosol backscattering was analyzed by a ceilometer to estimate the height of the planetary boundary layer.

The different meteorological data sources available in the same site represent a unique opportunity for the analysis of local circulation and for model validation in a Mediterranean area. For these reasons, five different WRF PBL schemes, two of which non-local and three local, are tested in this study. The whole measurement campaign is primarily considered for comparison with model outputs, but a discussion about the influence of the synoptic flow is also carried out. Simulations produced quite different results, depending on the PBL scheme, on the meteorological parameter, and on the atmospheric condition.

Near surface, all the WRF PBL schemes show a cold and moist bias, mostly during daytime, mainly as a consequence of overestimated breeze circulations; both for 2 m temperature and 2 m relative humidity, the two first order non-local schemes (ACM2 and YSU) are those that perform better. A general overestimation of the downward shortwave radiation is found, with better performance of the ACM2 scheme. 10 m wind speed is generally overestimated by WRF, being the QNSE scheme the one with the smallest bias. Regarding 10 m wind direction, the differences among the five schemes are negligible, with a general anticlockwise rotation of the simulated flow with respect to observations. For most of the parameters, QNSE is the scheme with the worst performance.

Considering the vertical wind profiles, the two non-local ACM2 and YSU schemes are, on average, those that perform better, both for wind speed and direction, while QNSE is the worst scheme. Generally, the model has a better performance for synoptic flow conditions, while it shows a worse skill in the simulation of breeze systems, which are more related to local forcings. The time evolution of the PBL heights confirms that YSU and ACM2 are closer to the observations, while QNSE significantly overestimates the mixing height. The important role of sensible heat fluxes is also analyzed, considering their time evolution.

In summary, non-local schemes appear to better represent the effects of the turbulence and the transport of heat and moisture in the planetary boundary layer. We believe that it is difficult to generalize these results, which are specific for the atmospheric conditions present during the campaign in Calabria region, characterized by the growth of the convective PBL under summertime, anticyclonic conditions. In agreement with previous studies showing similar atmospheric conditions (Banks et al., 2015, Banks et al., 2016, Pérez et al., 2006), we found that non-local schemes perform better in simulating surface parameters. It was supposed that this is due to the stronger vertical mixing (Bossioli et al., 2009), entrainment of air from above the PBLH (Cohen et al., 2015), and transport towards the surface associated with these schemes, which generated a different vertical development of the PBL compared to local PBL schemes (Hu et al., 2010).

On the other hand, Shin and Hong (2011) and Hariprasad et al. (2014) concluded that in stable conditions, the local TKE closure schemes show better performance in reproducing the vertical profiles of atmospheric variables. A larger dataset should be considered in the future to better quantify the performance of the WRF model in the presence of different synoptic conditions. At the same time, different test areas could be included in the study, in order to explore the generality of the present results, including also radiosoundings in the analysis of vertical profiles of thermodynamic variables.

Acknowledgments

This work is the result of a joint measurement campaign between ISAC-CNR and RISOE-DTU. Michael S. Courtney and Rozenn Wagner are particularly acknowledged for their active technical contribution. Special thanks to CRATI Scrl for the cooperation in the experimental campaign. We acknowledge both reviewers for the useful and constructive comments.

References

Avolio, E., Torcasio, R.C., Lo Feudo, T., Calidonna, C.R., Contini, D., Federico, S., 2016. Improvement of solar and wind forecasting in southern Italy through a multi-model approach: preliminary results. Adv. Sci. Res. 13, 69–73. http://dx.doi.org/10.5194/asr-13-69-2016.

Banks, R.F., Tiana-Alsina, J., Rocadenbosch, F., Baldasano, J.M., 2015. Performance evaluation of the boundary-layer height from lidar and the weather research and forecasting model at an urban coastal site in the North-East Iberian Peninsula. Bound.-Layer Meteorol. 157 (2), 265–292. http://dx.doi.org/10.1007/s10546-015-0056-2.

Banks, R.F., Tiana-Alsina, J., Baldasano, J.M., Rocadenbosch, F., Papayannis, A., Solomos, S., Tzanis, C.G., 2016. Sensitivity of boundary-layer variables to PBL schemes in the WRF model based on surface meteorological observations, lidar, and radiosondes during the HygrA-CD campaign. Atmos. Res. 176–177, 185–201. http://dx.doi.org/10.1016/j.atmosres.2016.02.024.

Bolle, H.J., 2003. Mediterranean Climate — Variability and Trends. Springer-Verlag, Berlin.

Borge, R., Alexandrov, V., del Vas, J.J., Lumbreras, J., Rodriguez, E., 2008. A comprehensive sensitivity analysis of the WRF model for air quality applications over the Iberian Peninsula. Atmos. Environ. 42, 8560–8574.

Bossioli, E., Tombrou, M., Dandou, A., Athanasopoulou, E., Varotsos, K.V., 2009. The role of planetary boundary-layer parameterizations in the air quality of an urban area with complex topography. Bound.-Layer Meteorol. 131, 53–72. http://dx.doi.org/10.1007/s10546-009-9349-7.

Breuer, H., Ács, F., Horváth, Á., Németh, P., Rajkai, K., 2014. Diurnal course analysis of the WRF-simulated and observation-based planetary boundary layer height. Adv. Sci. Res. 11, 83–88. http://dx.doi.org/10.5194/asr-11-83-2014.

Chou, M.-D., Suarez, M.J., 1999. A solar radiation parameterization for atmospheric studies. In: NASA Technical Report 104606, pp. 40 15 (June).

Cohen, A.E., Cavallo, S.M., Coniglio, M.C., Brooks, H.E., 2015. A review of planetary boundary layer parameterization schemes and their sensitivity in simulating southeastern U.S. cold season severe weather environments. Weath. Forecast 30 (3), 591–612. http://dx.doi.org/10.1175/WAF-D-14-00105.1.

Colacino, M., Conte, M., Piervitali, E., 1997. Elementi di climatologia della Calabria. IFA-CNR, Rome 197 pp.

Draxl, C., Hahmann, A.N., Peña, A., Giebel, G., 2014. Evaluating winds and vertical wind shear from weather research and forecasting model forecasts using seven planetary boundary layer schemes. Wind Energ. 17, 39–55. http://dx.doi.org/10.1002/we.1555.

Dudhia, J., 1993. A non-hydrostatic version of the Penn State-NCAR mesoscale model: validation tests and simulation of an Atlantic cyclone and cold front. Mon. Weather Rev. 121, 1493–1513.

Emeis, S., Schäfer, K., 2006. Remote sensing methods to investigate boundary-layer structures relevant to air pollution in cities. Bound.-Layer Meteorol. 121, 377–385.

Emeis, S., Schäfer, K., Münkel, C., 2008. Surface-based remote sensing of the mixing-layer height — a review. Meteorol. Z. 17, 621–630.

Endlich, R.M., Ludwig, F., Uthe, E.E., 1979. An automated method for determining the mixing depth from lidar observations. Atmos. Environ. 13, 1051–1056.

Eresmaa, N., Karppinen, A., Joffre, S.M., Räsänen, J., Talvitie, H., 2006. Mixing height determination by ceilometer. Atmos. Chem. Phys. 6, 1485–1493.

Federico, S., Bellecci, C., Colacino, M., 2003a. Numerical simulation of crotone flood: storm evolution. Il Nuovo Cimento C 26 (C), 357–371.

Federico, S., Bellecci, C., Colacino, M., 2003b. Quantitative precipitation of the Soverato flood: the role of orography and surface fluxes. Il Nuovo Cimento C 26 (C), 7–22.

Federico, S., Avolio, E., Bellecci, C., Lavagnini, A., Colacino, M., Walko, R.L., 2008. Numerical analysis of an intense rainstorm occurred in southern Italy. Nat. Hazards Earth Syst. Sci. 8, 19–35. http://dx.doi.org/10.5194/nhess-8-19-2008.

Federico, S., Pasqualoni, L., Sempreviva, A.M., De Leo, L., Avolio, E., Calidonna, C.R., Bellecci, C., 2010. The seasonal characteristics of the breeze circulation at a coastal Mediterranean site in South Italy. Adv. Sci. Res. 4 (47–56), 2010. http://dx.doi.org/10.5194/asr-4-47-2010.

Floors, R., Vincent, C.L., Gryning, S.E., Peña, A., Batchvarova, E., 2013. The wind profile in the coastal boundary layer: wind lidar measurements and numerical modelling. Bound.-Layer Meteorol. 147, 469–491.

Gascon, E., Laviola, S., Merino, A., Miglietta, M.M., 2016. Analysis of a localized flash-flood event over the central Mediterranean. Atmos. Res. 182, 256–268. http://dx.doi.org/10.1016/j.atmosres.2016.08.007.

Hariprasad, K.B.R.R., Srinivas, C.V., Bagavath Singh, A., Vijaya Bhaskara Rao, S., Baskaran, R., Venkatraman, B., 2014. Numerical simulation and intercomparison of boundary layer structure with different PBL schemes in WRF using experimental observations at a tropical site. Atmos. Res. 145, 27–44.

Holton, J.R., 2004. Introduction to Dynamic Meteorology, fourth ed. Elsevier 535 pp.

Hong, S.Y., Noh, Y., Dudhia, J., 2006. A new vertical diffusion package with an explicit treatment of entrainment processes. Mon. Weather Rev. 134, 2318–2341.

Hong, S.Y., Pan, H.L., 1996. Nonlocal boundary layer vertical diffusion in a medium-range forecast model. Mon. Weather Rev. 124, 2322–2339.

Hong, Song-You, Dudhia, Jimy, Chen, Shu-Hua, 2004. A revised approach to ice microphysical processes for the bulk parameterization of clouds and precipitation. Mon. Weather Rev. 132, 103–120.

Hu, X.-M., Nielsen-Gammon, J.W., Zhang, F., 2010. Evaluation of three planetary boundary layer schemes in the WRF model. J. Appl. Meteorol. Climatol. 49, 1831–1844. http://dx.doi.org/10.1175/2010JAMC2432.1.

Iacono, M.J., Delamere, J.S., Mlawer, E.J., Shephard, M.W., Clough, S.A., Collins, W.D., 2008. Radiative forcing by long–lived greenhouse gases: calculations with the AER radiative transfer models. J. Geophys. Res. 113, D13103.

Janjic, Z., 1990. The step-mountain coordinate: physical package. Mon. Weather Rev. 118 (7), 1429–1443.

Janjic ZI, 2002. Nonsingular implementation of the Mellor–Yamada level 2.5 scheme in the NCEP meso model. NCEP office note 437, 61 pp.

Jiménez, P.A., Dudhia, J., 2012. Improving the representation of resolved and unresolved topographic effects on surface wind in the WRF model. J. Appl. Meteorol. Climatol. 51, 300–316.

Johns, R.H., Doswell III, C.A., 1992. Severe local storms forecasting. Wea. Forecasting 7, 588–612.

Kain, John S., 2004. The Kain–Fritsch convective parameterization: an update. J. Appl. Meteorol. 43, 170–181.

Kim, Y., Sartelet, K., Raut, J.C., Chazette, P., 2013. Evaluation of the weather research and forecast/urban model over greater Paris. Boundary-Layer Meteorol 149, 105. http://dx.doi.org/10.1007/s10546-013-9838-6.

Kleczek, M.A., Steeneveld, G.J., Holtslag, A.A.M., 2014. Evaluation of the weather research and fore- casting mesoscale model for GABLS3: impact of boundary-layer schemes, boundary conditions and spin-up. Bound.-Layer Meteorol. http://dx.doi.org/10.1007/s10546-014-9925-3.

Lara-Fanego, V., Ruiz-Arias, J.A., Pozo-Vazquez, D., Santos-Alamillos, F.J., Tovar-Pescador, J., 2012. Evaluation of the WRF model solar irradiance forecasts in Andalusia (southern Spain). Sol. Energy 86, 2200–2217.

Melfi, S.H., Spinhirne, J.D., Chou, S.-H., Palm, S.P., 1985. Lidar observations of vertically organized convection in the planetary boundary layer over the ocean. J. Clim. Appl. Meteorol. 24, 806–821.

Miglietta, M.M., Zecchetto, S., De Biasio, F., 2013. A comparison of WRF model simulations with SAR wind data in two case studies of orographic lee waves over the Eastern Mediterranean Sea. Atmos. Res. 120–121, 127–146. http://dx.doi.org/10.1016/j.atmosres.2012.08.009.

Münkel, Räsänen, 2004. New optical concept for commercial lidar ceilometers scanning the boundary layer. In: Proc. SPIE 5571, Remote Sensing of Clouds and the Atmosphere IX. 364 November 30, 2004 http://dx.doi.org/10.1117/12.565540.

Nakanishi, M., Niino, H., 2006. An improved Mellor–Yamada level-3 model: its numerical stability and application to a regional prediction of advection fog. Boundary-Layer Meteorol 119, 397–407.

Pérez, C., Jiménez, P., Jorba, O., Sicard, M., Baldasano, J.M., 2006. Influence of the PBL scheme on high-resolution photochemical simulations in an urban coastal area over the Western Mediterranean. Atmos. Environ. 40 (27), 5274–5297.

Pleim, J.E., 2007. A combined local and non-local closure model for the atmospheric boundary layer. Part 1: model description and testing. J. Appl. Meteorol. Climatol. 46, 1383–1395.

Shin, H.H., Hong, S.-Y., 2011. Intercomparison of planetary boundary-layer parameterizations in the WRF model for a single day from CASES-99. Boundary-Layer Meteor. 139, 261–281. http://dx.doi.org/10.1007/s10546-010-9583-z.

Sicard, M., Pérez, C., Comeron, A., Baldasano, J.M., Rocaden-Bosch, F., Schafer, K.P., Comeron, C., Carleer, A.M.R., Picard, R.H., 2004. Determination of the mixing layer height from regular lidar measurements in the Barcelona area. In: Remote Sensing of Clouds and the Atmosphere VIII. Proceedings of SPIE 5235. pp. 505–516 Bellingham, WA, USA.

Skamarock, W.C., Klemp, J.B., Dudhia, J., Gil, D.A., Barker, D.M., Duda, M.G., Huang, X.-Y., Wang, W., Powers, J.G., 2008. Description of the Advanced Research WRF Version 3. National Center for Atmospheric Research. Boulder, Colorado, USA.

Srikanth, M., Satyanarayana, A.N.V., Srinivas, C.V., Kumar, M., 2015. Mesoscale atmospheric flow-field simulations for air quality modelling over complex terrain region of Ranchi in eastern India using WRF. Atmos. Environ. 107, 315–328.

Stensrud, D.J., 2007. Parameterization Schemes: Keys to Understanding Numerical Weather Prediction Models. Cambridge University Press 459 pp.

Steyn, D.G., Baldi, M., Hoff, R.M., 1999. The detection of mixed layer depth and entrainment zone thickness from lidar backscatter profiles. J. Atmos. Ocean. Technol. 16, 953–959.

Stull, R.B., 1988. An Introduction to Boundary Layer Meteorology. Kluwer Academic Publishers, Dordrecht, Boston, London 666 pp.

Sukoriansky, S., Galperin, B., Perov, V., 2005. Application of a new spectral theory of stably stratified turbulence to atmospheric boundary layers over sea ice. Boundary-Layer Meteorol 117 (2), 231–257.

Tewari, M., Chen, F., Wang, W., Dudhia, J., LeMone, M.A., Mitchell, K., Ek, M., Gayno, G., Wegiel, J., Cuenca, R.H., 2004. Implementation and Verification of the Unified NOAH Land Surface Model in the WRF Model. 20th Conference on Weather Analysis and Forecasting/16th Conference on Numerical Weather Prediction. pp. 11–15.

Trigo, I.F., Davies, T.D., Grant, R.B., 1999. Objective climatology of cyclones in the Mediterranean region. J. Clim. 12, 1685–1686.

Wilks, D.S., 2011. Statistical Methods in the Atmospheric Science, third ed. Elsevier Academic Press 704 pp.

Xie, B., Fung, J.C.H., Chan, A., Lau, A., 2012. Evaluation of nonlocal and local planetary boundary layer schemes in the WRF model. J. Geophys. Res. 117, D12103.

Zhang, H., Pu, Z., Zhang, X., 2013. Examination of errors in near-surface temperature and wind from WRF numerical simulations in regions of complex terrain. Weather Forecast. 28, 893–914.

Zhong, S., In, H., Clements, C., 2007. Impact of turbulence, land surface, and radiation parameterizations on simulated boundary layer properties in a coastal environment. J. Geo-Phys. Res. 112, D13110http://dx.doi.org/10.1029/2006JD008274.